ChemistrySelect

Research Article
doi.org/10.1002/slct.202203877

Chemistry Europe
European Chemical Societies Publishing

www.chemistryselect.org

Propitious Indazole Compounds as β-ketoacyl-ACP Synthase Inhibitors and Mechanisms Unfolded for TB Cure: Integrated Rational Design and MD Simulations

Adeniyi T. Adewumi,[a, b] Wande M. Oluyemi,[b, c, e] Yemi A. Adekunle,[b, e, g] Nonhlanhla Adewumi,[b, d, f] Mohamed Issa Alahmdi,[h] Mahmoud E. S. Soliman,*[a] and Nader E. Abo-Dya[i, j]

Mycobacterium tuberculosis β-ketoacyl-ACP synthase I (KasA) involves in mycolic acid biosynthesis for cell wall maintenance; hence, it is a critical target in TB drug design. Thiolactomycin (TLM) and derivatives are the known standard KasA enzyme activity inhibitors. However, TLM analogues have poor activity against KasA protein. Indazole sulphonamide chemotype (JSF-3285/JFX) was recently reported as a promising KasA enzyme inhibitor. JSF-3285 mechanism is unclear; thus, it provides a means for designing KasA inhibitors. This study unfolds six hits as unprecedented KasA inhibitors. The inhibitory mechanisms of the screened compounds were investigated and compared with a standard inhibitor (TLM) using integrated molecular informatics and dynamics. JFX, M1, M2, and M5 molecules showed stronger interactions with KasA, having binding energy (kcal/mol) of −44.05, −41.52, −39.51, and −35.9, respectively, against −11.69 for TLM. Molecules showed good predicted inhibitory constants, drug-likeness, ADME, and synthetic accessibility. KasA complex C-α atoms RMSD and RMSF showed stable and erratic fluctuations compared to apo KasA. The findings provide potential antimycobacterial lead-like molecules for future TB drugs.

Introduction

Tremendous global efforts and strategies have had a remarkable impact on stopping the TB pandemic, especially from 2000 to 2020.[1] Despite the landmark reduction, tuberculosis cases and deaths continue to increase due to inherent drug resistance, COVID-19 emergence, and the fall in global funding for treatment strategies. *Mycobacterium tuberculosis* is successful in its virulence, survival, and drug-resistance activities.[2] Drug resistance and coronavirus infectious disease, first identified in the 2019 (COVID-19) pandemic, has continued to reverse the years of progressive TB service and burden reduction.[3,4] Unfortunately, the drugs used to treat multidrug resistance tuberculosis (MDR TB) have also been resisted by the TB pathogen. For instance, MDR strain resistance has been reported in Rifampicin, Isoniazid, and Fluoroquinolones.[5] Many people have been newly diagnosed with TB compared to the previous years. This increase in TB diagnosis and lack of adequate treatment has increased deaths; 1.3 million TB deaths among HIV-negative people from 1.2 million and 214000 deaths among HIV-positive people from 209000 in 2019.[1] Moreover, the COVID-19 impact caused a sharp fall in the Number of people being provided drug-resistant treatment, TB

[a] *Dr. A. T. Adewumi, Prof. M. E. S. Soliman*
Molecular Bio-computation and Drug Design Laboratory, School of Health Sciences, University of KwaZulu-Natal, Westville Campus, Durban 4001, South Africa
E-mail: soliman@ukzn.ac.za
[b] *Dr. A. T. Adewumi, Dr. W. M. Oluyemi, Y. A. Adekunle, N. Adewumi*
Research Laboratories for Rational Design of Drugs and Biomaterials, Isiphephelo Court, Tsakane, 1550, Brakpan, Johannesburg East Rand, Gauteng, South Africa
[c] *Dr. W. M. Oluyemi*
Department of Pharmaceutical and Medicinal Chemistry, College of Pharmacy, Afe Babalola University, Ado-Ekiti, Ekiti State, Nigeria
[d] *N. Adewumi*
Department of Chemistry, Faculty of Applied and Computer Sciences, Vaal University, Vanderbijl Park, South Africa
[e] *Dr. W. M. Oluyemi, Y. A. Adekunle*
Laboratory for Natural Products and Biodiscovery Research, Pharmaceutical Chemistry Department, Faculty of Pharmacy, University of Ibadan, Nigeria
[f] *N. Adewumi*
Chemical research Laboratory, BetaChem Pty Ltd, ERF5 Producta Road, Driemanskap, Heidelberg, 1441, Gauteng, South Africa
[g] *Y. A. Adekunle*
Centre for Natural Products Discovery (CNPD), School of Pharmacy and Biomolecular Sciences, Liverpool John Moores University, Liverpool L3 3AF, United Kingdom.
[h] *Dr. M. I. Alahmdi*
Department of Chemistry, Faculty of Science, University of Tabuk, Tabuk, 7149, Saudi Arabia
[i] *Dr. N. E. Abo-Dya*
Department of Pharmaceutical Chemistry, Faculty of Pharmacy, Tabuk University, Tabuk, 71491, Saudi Arabia.
[j] *Dr. N. E. Abo-Dya*
Department of Pharmaceutical Organic Chemistry, Faculty of Pharmacy, Zagazig University, Zagazig, 44519 Egypt,

Supporting information for this article is available on the WWW under https://doi.org/10.1002/slct.202203877

preventive treatment, and global funding allocation towards diagnosis, prevention, and treatment. On the other hand, malnutrition, smoking, and alcohol use remain deadly impacting factors[2] which people have refused to reduce or stop.

β-ketoacyl-ACP synthase I (Kas A) protein is critical for the cellular synthesis of fatty acid synthase II (FAS II) complex mycolic acid. KasA is one of the crucial enzymes involved in the biosynthesis of macromolecules in the cell wall. The protein represents the enzymatic cyclization of short-chain fatty acids (C_{20-26}) to long-chain meromycolic acids (C_{50-56}), which condense with C26 fatty *Pks13* to produce branched mycolic acids. It uses a ping-pong-like mechanism to catalyze a condensation reaction between malonyl-AcpM and the growing acyl chain. The N-terminal of KasA protein comprises residues 2–259, while the C-terminal comprises residues 260–416. The enzyme structure has 414 amino acid residues, which all together form an α-β-α-β-α of five-layered structure. The core domain catalytic triad of KasA includes CYS170, HIS311, and HIS345, located in the N-terminal. The remaining catalytic residues are present in the C-terminal region.[6]

The natural product thiolactomycin (TLM) and its derivatives are still known standard inhibitors of KasA enzyme activity.[7–9] However, TLM and its analogues have poor inhibitory activities against *Mycobacterium tuberculosis* whole-cell;[9] the minimum inhibitory concentrations of TLM and Platensimycin are 142 μM and 27 μM, respectively. TLM is a slow-onset inhibitor that binds to the CYS171 residue of the KasA enzyme. Hence, it results in structural changes in the movement of α5 and α6 that initiate the binding of malonyl-AcpM to TLM.[10] Moreover, GlaxoSmithKline recently reported that an indazole sulphonamide compound (JSF-3258) inhibits KasA in vitro and a mouse model with a good pharmacokinetic profile.[12] Despite the remarkable results, JSF-3285 is still in the preclinical stage. Moreover, this compound binds to the phospholipid (PL) pocket of KasA rather than binding to the CYS171, making its mechanism of action unclear.

The drug design of small molecule inhibitors often requires various screening approaches, including experimental and computational, to obtain essential information that facilitates drug development.[13,14] *In silico* molecular modelling techniques have continued to gain importance in drug design and development, without exception in designing antitubercular agents with different functional biological receptors.[14] Furthermore, there seem to be limited reports on the dynamics studies of KasA-inhibitor using molecular dynamics simulations and MMGB(PB)SA. Therefore, several multi-computational methods were used in this study to answer critical problem statements that can enhance the development of antimycobacterial agents. We aimed to identify more potent antitubercular molecules against KasA protein using a *de novo* approach, pharmacophore-based virtual screening,[15] molecular docking,[16] and integrated molecular dynamics simulations.[17–19] We further explored the molecular inhibitory constant of the proposed potential novel inhibitors and their binding free energy calculations,[20] and absorption, distribution, metabolism, and excretion (ADME) predictions.[18] The physicochemical properties, including the ADME of the six molecules, have been determined.[21] Structure-based virtual screening (SBVS) is a cost-economical tool that identifies and prioritizes ligands for *in vitro* and *in vivo* profiling. Thus, SBVS provides a potential platform for novel Kas A inhibitors. Therefore, the technique is considered an integral part of drug design used early in drug discovery campaigns to search for a chemical compound for novel bioactive molecules against a specific drug target. This study reported the ADME's pharmacokinetics (PK) and pharmacodynamics (PD) profiles of the screened inhibitors.[21,22] The compounds have antitubercular activity potentials that will be explorable in further investigations.

Computational methodology

Retrieval and preparation of β-ketoacyl-ACP synthase (*KasA*) protein

The *Mycobacterium tuberculosis* β-ketoacyl-ACP synthase (KasA) X-ray monomer crystal structure, co-crystallized with JSF-3285 (JFX), was obtained from the RCSB Protein Data Bank (accession codes, 6P9L[12] and resolutions, 2.31 Å). JSF-3285 structure was chosen on its good X-ray quality, crystallographic ligand similarity to indazole compound 5G,[6] and dynamics and binding energy studies. Subsequently, receptor and inhibitor JSF-3285 were prepared using the Chimeratool-1.14[23,24] and the AutoDockTool-1.5.6[25] and optimized (using the Molegro Molecular Viewer-2.5)[26] for molecular dynamic (MD) simulation study. The unbound and ligand-bound systems' preparation involves removing nonstandard molecules, including water, GOL, IPA, and sodium.[27]

Pharmacophore modeling of JFX-bound *KasA* protein

First, the inhibitor JSF-3285 was simulated at the substrate-binding site of the β-ketoacyl synthase I enzyme for 40 ns to generate a bound conformation of the ligand (Figure 1A). A per-residue energy decomposition study was used to identify the amino acids that contributed the highest energy in the binding of the inhibitor. The pharmacophoric groups interacting with the highly contributing residues were used to build the model. The model criteria include the molecular weight <500 Da, rotatable bonds <6, hydrogen bond donor <5, and hydrogen bond acceptor <10. The model pharmacophores include the pyrazole N═O (acceptor), a sulphonamide S═O (acceptor), and a fluorine (acceptor). A sulphonamide nitrogen (donor), hydrophobic benzene and hydrophobic pyrazole ring groups were also considered. The pyrazole nitrogen, sulphonamide oxygen, and sulphonamide NH formed conventional H-bonds with the backbones of GLY115, GLU197, and SER344, respectively (Figure 1B). The pyrazole ring formed hydrophobic interactions, including amide-pi stacked and pi-alkyl with LEU114, while the pyrazole $-CH_3$ group formed alkyl interaction with the sidechain of LEU114. In addition, the drug-likeness of the molecules was investigated using Lipinski's five rules.

Structure-based virtual screening

Molecular database: Selection and preparation

The in-house structure-based virtual screening protocol was used to identify drug-like hits. An *in silico* modeling study was carried out over various freely available chemical compounds in the ZINCPharmer chemical library (http://zincpharmer.csb.pitt.edu/pharmer.html) chosen for virtual screening by uploading the ligand

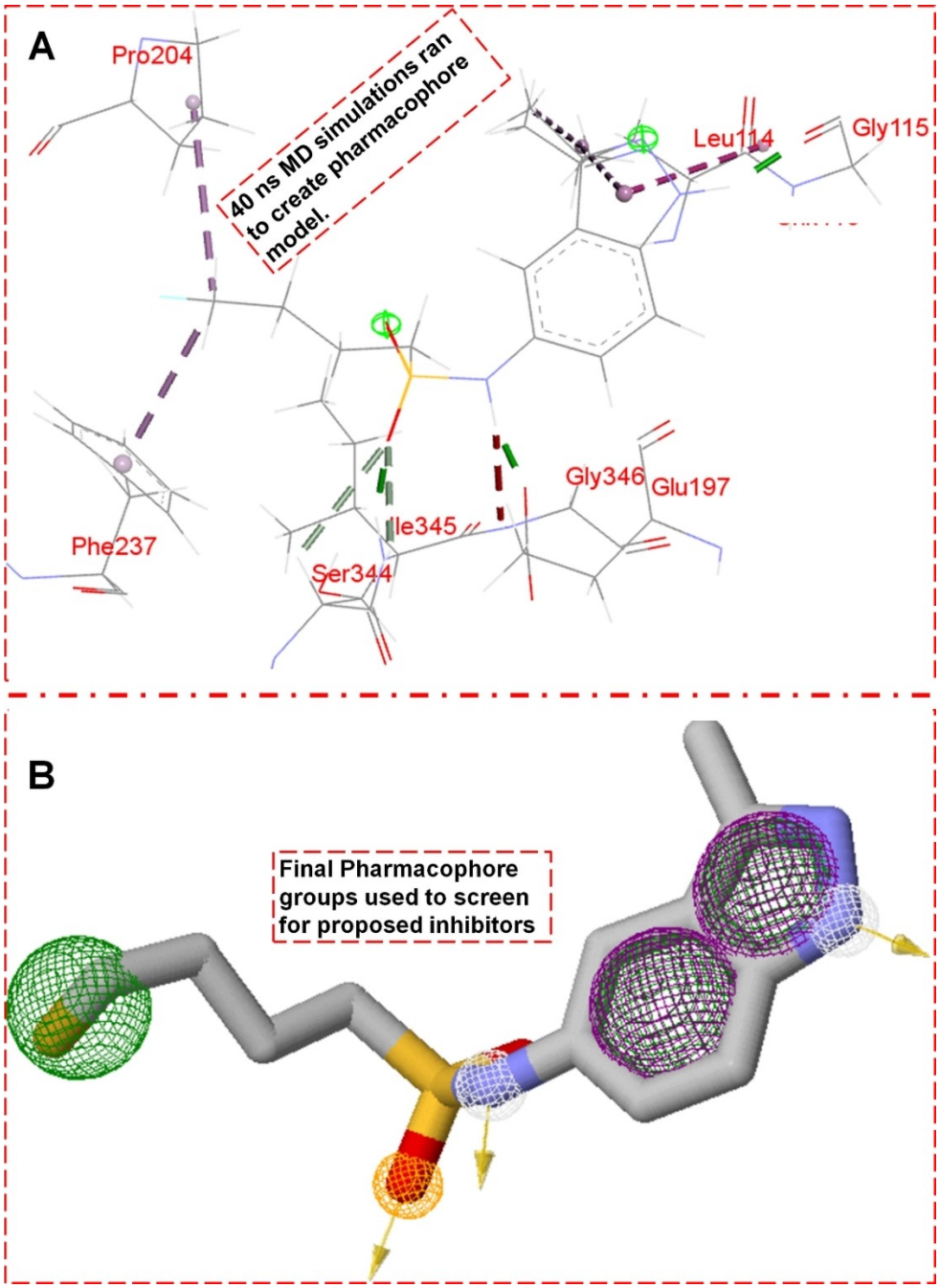

Figure 1. (A) The 40 ns MD simulation pharmacophore model, (B) Final pharmacophore groups were used to screen the proposed inhibitors M1, M2, M3, M4, M5, and M6.

to the library.[28] A query of the chemical dataset was downloaded as the structural data format (SDF) and converted into another file extension (.pdb and mol2) using Open Label, an open-source tool for file compatibility conversion.[29] The above-selected chemical library, consisting of 817 unique compounds, was obtained for virtual screening. The compounds' polar functional groups are critical for hit-to-lead identification and optimization and structure-based and fragment-based drug design. The compounds were prepared in the ADT[25] and saved as PDBQT formats to enable compatibility with the AutoDock Vina[30] format.

Molecular docking

The ligands were differentiated by molecular docking based on the compounds' geometry to bind to the protein's active site.[31] The *Mycobacterium tuberculosis* KasA protein was prepared for docking calculation using the AutoDockTool (ADT)-1.5.6. All nonstandard molecules, including water, were removed from the crystal structure, and the appropriate Number of polar hydrogen atoms was added to the enzyme. Moreover, the Gasteiger charges were assigned to the KasA protein structure.[32,33] After that, the docking was performed using a grid box of dimension 70 Å×70 Å×70 Å in

ADT, covering the protein structure while keeping the center of the binding site coordinates at −18.770, 11.801, 22.843, respectively. However, the detailed information regarding the grid box and prepared enzymes and ligands were contained in a configuration file, a text file extension required for docking calculations in ADT. The protein structure was kept rigid, while the 817 ligands were fully flexible during docking. The CHPC Lengau server Linux-based installed Autodock Vina was used. (http://www.chpc.ac.za/index.php/resources/lengau-cluster). The molecular docking results of prospective 817 compounds were selected based on the highest binding energy range from −10.0 to −10.4 after the docking calculations were completed for the best active antitubercular compound. The protein-ligand complexes were critically examined to screen out the low binding mode poses (below −10.0) and subsequently selected for further modelling analysis. The selected complexes were visualized using the Discovery Studio-v21.1.0.20298 tool to analyze the molecular interaction profiles in 3-dimensional space.

Molecular dynamics simulations

Although, some molecular docking results produce good complex geometric conformations or poses. However, the literature has shown that molecular docking or short MD simulations of molecular systems often lead to instability. Therefore, the stability of the conformations of such complexes can be validated by carrying out molecular dynamics (MD) simulations for a long time to stabilize the system. Hence, the MD studies for the most favourably proposed inhibitor-KasA complexes were carried out to validate the docking approach used in this study. The MD simulation of the screened molecule-bound KasA complexes was run for 200 ns.

The molecular dynamics simulation was carried out using the Amber GPU version of the PMEMD engine provided by the AMBER18 package at the Lengau CHPC (http://www.ambermd.org).[34] The inhibitors-KasA complexes were described with the AMBER18 FF18SB force field variant.[35,36] Using the combined procedures, we applied the antechamber package to obtain the atomic partial charges for the ligands, involving restrained electrostatic potential (RESP) and the General Amber Force Field (GAFF).[36] The Amber 18 leap module was used to add the hydrogen atoms, sodium (Na^+), or chloride (Cl^-) counter ions to the system for neutralization, depending on the complex charge state. The complexes, implicitly, were suspended within an orthorhombic box of TIP3P water molecules to contain all atoms within 12 Å of any box edges.[37] The systems were partially minimized for 2500 steps with 500 kcal/mol Å^2 restraint potential, and 5000 steps of full minimization were carried out without restraint using the conjugate algorithm. The heating step was performed in a canonical ensemble condition (*NVT*) by gradually heating the systems from 0 to 300 K for 5 ps with fixed atoms and volumes. The solute systems were imposed with 10 kcal/mol Å^2 potential harmonic restraint and 1.0 ps^{-1} collision frequency. While keeping the operating temperature, T (300° K), constant, we equilibrate the protein systems for 1 ns (500 000 steps).

The Number of atoms and pressure were kept constant to keep an isobaric isothermal ensemble (NPT). The pressure of the systems was kept at 1 bar using the Berendsen barostat.[16,38] We used the SHAKE algorithm to construct the hydrogen atom bonds. At every 1 ps, the coordinates and trajectories were printed and analyzed with the AMBER18 GPU PTRAJ module.

After the MD simulations, the root mean square deviation (RMSD) and the root mean square fluctuation (RMSF)[16] of the free and bound KasA protein were computed to investigate the stability and flexibility of the systems, respectively. In addition, we computed the principal component (PCA) of the protein systems to explore the degree of residual atomic displacement. Further details on the post-MD computation RMSD,[19] RMSF,[39] and PCA[40] parameters are available in the literature.

Binding free energy

The binding free energies were computed using the Molecular Mechanics Generalized-Born Surface Area method (MMGBSA)[41] to obtain the binding affinities between the free protein and the ligands. The free energy was calculated based on the average of 10 000 snapshots extracted from a 40 ns trajectory. The computed binding free energy (ΔG) of the complex systems involved the energy contributions by the inhibitors and protein was obtained from the following mathematical relationships (equations i–v):[42]

$$\Delta G_{bind} = G_{complex} - G_{protein} - G_{inhibitor} \quad \text{(i)}$$

$$\Delta G_{bind} = E_{gas} + G_{sol} - TS \quad \text{(ii)}$$

$$E_{gas} = E_{int} + E_{vdw} + E_{ele} \quad \text{(iii)}$$

$$G_{sol} = G_{GB} + G_{SA} \quad \text{(iv)}$$

$$G_{SA} = \gamma SASA \quad \text{(v)}$$

Further information regarding the binding free energy calculations using the MMGBSA methods has been reported in our published literature.[43]

Hits' drug-likeness: Pharmacokinetics and pharmacochemical evaluations

The compounds were subjected to online software, SwissADME, to predict the screened compounds based on parameters, including drug-likeness and pharmacokinetics. In addition, the physicochemical descriptors of the compounds were predicted.

Results and discussion

Virtual screening drug design

In searching for effective compounds with promising inhibitory activities, we used the structure-based drug design, a critical tool in drug discovery, aiding fast and cost-economical lead discovery and optimization.[44] The structures of the *Mtb* KasA co-crystallized with JFX (PDB code 6P9L) and the co-crystallized *Mtb* KasA with Thiolactomycin (TLM) (accession code 2WGG)[45] were used in this study. The JFX was chosen for its promising experimental inhibitory activity and used for model generation. In contrast, the study of the *Mtb* KasA activity's inhibition by TLM was done only to emphasize and confirm the compound's inactivity against the pathogen and compare it with JFX at the level of drug potentiality. Most importantly, the mechanism of action of the JFX and TLM are different because each compound binds to a different active site. Thus, the binding

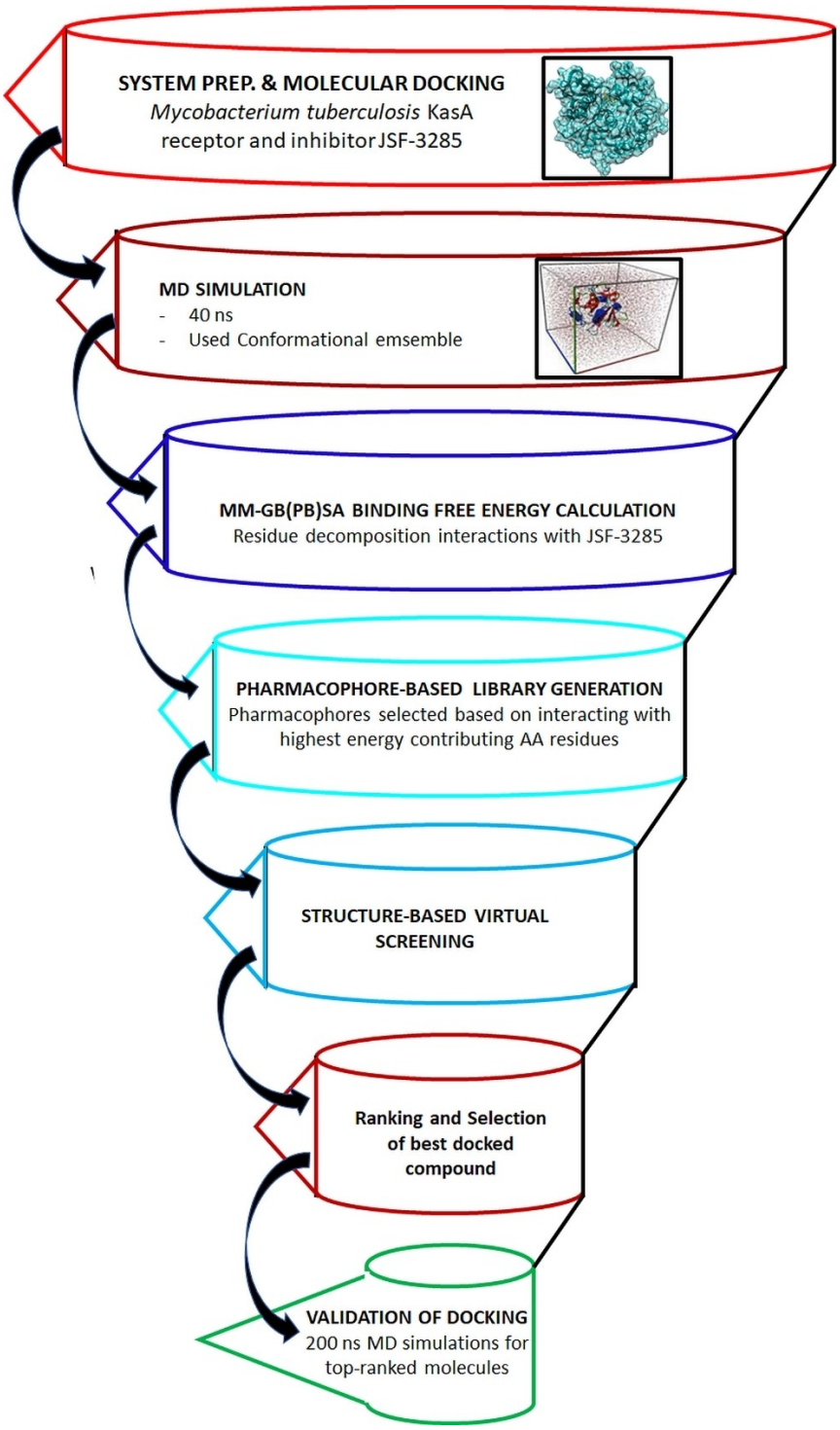

Figure 2. Schematic illustration of the structure-based virtual screen strategy in this study. Each step is detailed: preparation of KasA enzyme, JSF-3285, and TLM, retrieval of antimycobacterial compounds from the ZINCPharmer (817 molecules). Moreover, the initial selection of 817 inhibitors was performed and checked for drug-likeness using Lipinski's rule of five. Thirteen (13) KasA inhibitors were screened considering acceptable pharmacokinetics profile (ADMET screening) and synthetic accessibility testing. The final six (6) promising KasA enzyme inhibitors were obtained and taken through bioactivity prediction and quality assessment. Validation of docking investigated by performing the molecular dynamics simulation and binding free energy analysis (MMGB(PB) SA) studies of the six inhibitors were performed.

affinities of the two compounds were not relatively compared. Therefore, the threshold binding affinity of −10.0 kcal was chosen to select the screened molecules based on the minimum lowest energy ranking rather than comparing with TLM binding energy. Moreover, our recently accepted manuscript on the molecular dynamics and binding free energy

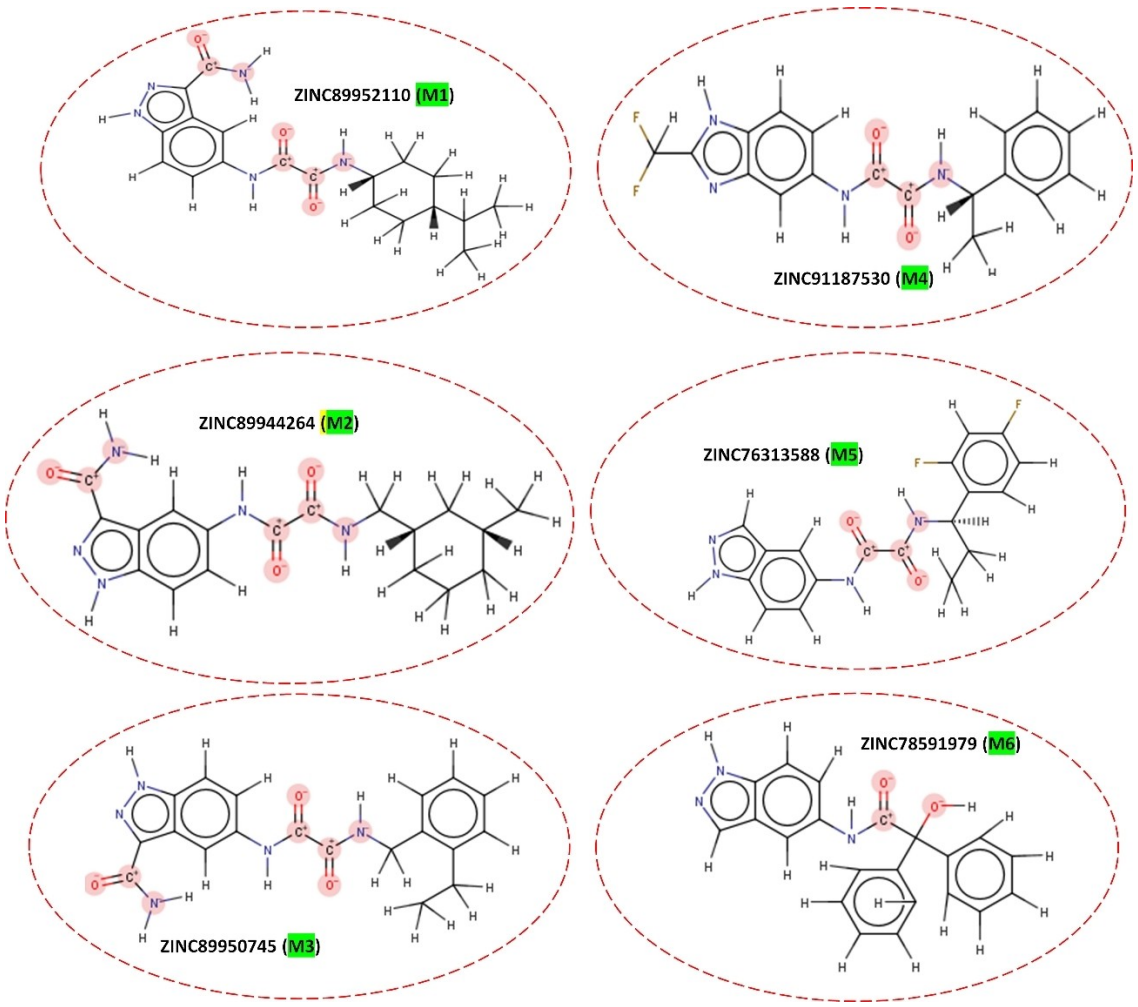

Figure 3. The 2-Dimensional structure of the proposed *Mycobacterium tuberculosis* KasA enzyme inhibitor

findings of the JFX-KasA complex, as a part, is in publication process stage by the *Current Topics in Medicinal Chemistry Journa*l. Of importance, we compared the results of JFX-KasA complex with the screened molecules. Nevertheless, we briefly compared the stability, flexibility, and the binding free energy results of JFX-bound KasA with the screened molecules in this study. Figure 2 provides this study's schematic steps of the SBVS strategy.

Eight hundred and seventeen (817) molecules from the ZINCPharmer chemical library, JSF-3285, and TLM were docked to each KasA active site system. The molecular binding affinity of all the compounds was obtained. The molecular docking method is pivotal to this modern-day rational drug design research. The technique identifies promising drug-like molecules from large chemical databases with high binding affinity for a target such as KasA protein. Hence, molecular docking was used in this study.

The prospective antimycobacterial molecules in the downloaded dataset were docked to the target using the AutoDock Vina program.[30] The binding affinity distribution of the 817 compounds complexed with *KasA* was obtained. The chemical space of the molecules was narrowed down after molecular docking calculations by considering docked poses having binding energies ≥ -10.0, with the highest binding energy being -10.4.[46]

The binding affinities of the docked compounds were explored. The molecules that passed the criteria were merged, and duplicates were deleted. Altogether, 13 molecules were retained and subjected to further screening. The retaining 13 molecules were screened based on Veber's and Lipinski's rule of five RO5, allowing prediction and identification of drug-like characteristics of chemotype compounds. For several decades, the rules have been helpful in drug discovery to consider molecules possessing a significant likelihood of favourable drug absorption or permeation administered via the oral route. Lipinski's rule of five selects a drug-like candidate for oral administration. The criteria state that a molecule must possess H-bond donors ≤ 5, molecular weight ≤ 500, octanol-water partition coefficient < 5, and H-bond acceptors ≤ 10.[47,48] Veber stated that good oral bioavailability compounds would possess rotatable bonds (RTB) < 10 and polar surface area (PSA) < 140 Å[49,50] Interestingly, none of these 13 molecules violated

either rule. Therefore, all compounds were screened for a pharmacokinetics (Pk) study.

Considering the ADME results, 11 molecules showed low acceptable gastric intestinal (GI) absorption, while two compounds displayed high GI absorption. However, Table 2 provides the predicted GI absorption of the final molecules: M1, M2, M3, and M4 have low GI absorption, while M5 and M6 have high GI absorption. According to Lipinski's rule, a molecule with MW $<$ 500 (may not correlate with absorption), log $P<5$, HBD ≤ 5, and HBA ≤ 10 should have good GI absorption or an oral route of administration, the rules which the six molecules satisfied. In addition, Veber *et al.* have shown that an orally active drug with good GI absorption should have PSA $<$ 140 Å^2 and molecular rigidity (measured as the Number of Rotatable Bond ≤ 10). For these reasons, the molecules would have a chance of being bioavailable through the GI tract. However, several successful methods, including nano-formulation, etcetera, are reportedly used to improve the GI absorption of potential orally active compounds or drugs.[51–54]

In addition, synthetic accessibility Scores (SA score) of drug-like molecules should imply easy synthetic accessibility.[55] The high synthetic accessibility value indicates the difficulty of synthesizing. Hence, low SA scores are considered in medicinal/pharmaceutical chemistry research.[56] Considering the obtained ADME analysis, the distribution of synthetic accessibility of the 13 molecules showed that the scores of the molecules are easily synthetically accessible because the scores were <5. Only six (6) molecules were selected using solubility criteria, and the molecules were considered potentially interacting compounds or could exhibit inhibition against *Mycobacterium tuberculosis* KasA protein. Figure 3 shows the 2-D structures of the six molecules M1, M2, M3, M4, M5, and M6.

Analysis of molecular docking and binding affinities.

The binding affinities (BA) of the final proposed molecules of the KasA inhibit are given in Table 1. The BA of the 13 promising molecules showed a strong affinity towards the KasA enzyme compared to the 804 molecules with lower binding energies. However, the final proposed inhibitors, considering the subsequent pk and physicochemical screening, the first six molecules (M1, M2, M3, M4, M5, and M6) were the final proposed inhibitors.

Table 1. The 13 molecules with the highest docking binding affinity for the proposed KasA protein.

Molecule	ZINCPHARMER library name	Binding energy (kcal/mol)
M1	ZINC89952110	−10.4
M2	ZINC89944264	−10.3
M3	ZINC89950745	−10.3
M4	ZINC91187530	−10.1
M5	ZINC76313588	−10.0
M6	ZINC78591979	−10.0
M7	ZINC13728984	−10.0
M8	ZINC76239043	−10.2
M9	ZINC89944414	−10.2
M10	ZINC89953032	−10.3
M11	ZINC91187577	−10.0
M12	ZINC91212740	−10.0
M13	ZINC91210152	−10.1

Moreover, validating the docked structure with experimentally known drugs was impossible due to the lack of FDA-approved inhibitor binding to the active site (Phospholipid (PL) binding site). Therefore, we compared the remaining results with the unbound protein system.

The binding energy (BE) results in the molecular docking range from −10.0 to −10.4 (Table 3). However, the (BE) differences among the molecules appear insignificant but could be critical to inhibition. For instance, the difference between M1 and M6 is −0.4. It indicates that M1 is preferentially buried deeper in the binding socket than the M2, M3, M4, M5, and M6. Therefore, it provides an avenue for comparing the binding interactions in the subsequent analysis, i.e., the molecular dynamics simulations of the ligand-bound *KasA* protein.

Pharmacokinetics (Pk) and pharmacochemical evaluations

Quality assessment of the proposed KasA inhibitors

The analysis of the physicochemical properties of a chemical compound reveals its potential, whether it reaches the target site and attains the maximum plasma (therapeutic) concentration or not.[18,57] The screening further uncovered the degree of therapeutic activity of the chemical compounds when bound to the target's active site. Hence, the *in silico* physicochemical and Pk parameters of M1, M2, M3, M4, M5, and M6 (Table 2) were obtained from the SwissADME database source (http://www.swissadme.ch/). The molecular weights of the six *KasA* inhibitors range between approximately 326–446 g/mol. The polar surface areas (PSA, Å^2) of the proposed molecules M1, M2, M3, M4, M5, and M6 were 75.93, 75.93, 75.93, 34.14, 58.86, 41.76, respectively.

The topological surface area (TPSA) or polar surface area (PSA) is the sum of surface overall polar atoms or molecules such as oxygen, nitrogen, and their attached hydrogen atoms. PSA is a commonly used metric in medicinal chemistry to optimize the ability of a drug to permeate through a cell membrane or blood-brain. The PSA of a compound $>$ 140 Å^2 is poor for cell membrane permeation.[58] Moreover, a PSA $<$ 90 Å2 molecule permeates through the blood-brain.[59] These findings indicate that the molecules will permeate the cell membrane and thus the blood-brain. In addition, the PSA values of the molecules implied that they are orally active. Interestingly, all molecules showed good aqueous solubility, but M4 is more soluble than others.

To further ascertain the assessment of the compounds, the gastrointestinal absorption (GI) findings indicate that M5 and M6 will be more easily absorbable in the intestine than molecules M1-M4. The low synthetic accessibility values of the molecules confirmed that none of them may be difficult to synthesize. Moreover, we reported the drug-likeness behaviour of M1, M2, M3, M4, M5, and M6 as given in the bioavailability (BA) radar plot (Figure 4) to gain better insights into the potential therapeutic quality of the compounds. The BA radar

Table 2. Physicochemical parameters of the six proposed *Mtb* KasA protein inhibitors.

Parameters	M1 (−10.4)	M2 (−10.3)	M3 (−10.3)	M4 (−10.1)	M5 (−10.0)	M6 (−10.0)
Formula[a]	$C_{19}N_5O_3$	$C_{18}N_5O_3$	$C_{19}N_5O_3$	$C_{18}F_2N_4O_2$	$C_{18}F_2N_4O_2$	$C_{21}N_3O_2$
MW(g/mol)[b]	346.23	334.22	346.23	342.22	342.22	326.24
NHA[c]	27	26	27	26	26	26
NAHA[d]	0	0	6	12	6	12
NRB[e]	7	7	8	6	7	5
MR[f]	87.59	85.13	87.59	81.35	82.81	88.13
TPSA (Å^2)[g]	75.93	75.93	75.93	34.14	58.86	41.79
LogP[h]	0.08	0.06	0.14	-0.12	1.35	1.48
LogS[i]	−2.56	−2.30	−2.27	−1.85	−3.00	−3.29
SC[j]	Soluble	Soluble	Soluble	Very Soluble	Soluble	Soluble
GI[k]	Low	Low	Low	Low	High	High
BS[l]	0.55	0.55	0.55	0.55	0.55	0.55
SA[m]	4.31	4.31	3.34	2.72	3.63	3.71
vROF[n]	0	0	0	0	0	0

[a] Molecular Formula
[b] Molecular weight;
[c] Number of heavy atoms;
[d] Number of heavy aromatic atoms;
[e] Number of rotatable bonds;
[f] Molar refractivity;
[g] Topological polar surface area;
[h] Partition coefficient;
[i] Solubility;
[j] Solubility class;
[k] Gastrointestinal absorption;
[l] Bioavailability Score;
[m] Synthetic accessibility;
[n] Violation of Lipinski's rule of five.

plot showed various properties of the molecules, which include lipophobicity ((LIPO), rotatable bonds (FLEXI), and unsaturation (INSATU). The other properties are insolubility (INSOLU), polar surface area (POLAR), and molecular weight (SIZE). In addition, the plot indicated the recommendation value of each parameter; $-0.7 < \text{LIPO} < +5$, $0 < \text{FLEXI} < 9$, $0.25 < \text{INSITU} < 1$, $20 < \text{POLAR (Å}^2) < 130$, and $\text{SIZE} < 500$ g/mol. Inferentially, the radar plot revealed that the molecules possess acceptable drug-likeness properties. Figure 4 illustrates the plot of the bioavailability radar of the proposed KasA enzyme inhibitors.

Prediction of bioactivity of the final proposed KasA inhibitors

The bioactivity of screened compounds can be predicted by computing their inhibitory constant (K_i) in equation (vi) from the individual binding energy obtained from the molecular docking calculations.[60]

$$K_i = e^{-\Delta G/RT} \quad \text{(vi)}$$

K_i = inhibitory constant; ΔG = molecular docking binding energy; R = gas constant (1.987×10^{-3} kcal/k^{-mol}); and T = temperature (298.15 K).

The Low K_i value of a chemical compound strongly indicates a lead potentiality.[61,62] The proposed KasA inhibitors showed lead potential because the theoretical inhibitory constants are very low. Table 3 shows that the lead potentiality of the proposed KasA inhibitors can be arranged as M1, M2 = M3, M4, and M5 = M6 based on their calculated K_i values.

Apart from the predicted ligand inhibitory constant, parameters, including ligand efficiency (LE), LE scale (LE_{scale}), fit quality (FQ), and LE-dependent lipophilicity, were used to investigate the efficacy of the proposed KasA inhibitor in this study. LE (equation vii) allows the investigation of the lead-likeness of a molecule[63] and can be obtained as follows:

$$LE = \frac{-BE}{NHA} \quad \text{(vii)}$$

NHA = the Number of heavy atoms contained in the molecule; BE = binding energy.

However, C. H. Reynolds and R. C. Reynolds reported that the LE depends on the molecular size.[64] This shortcoming led to the proposed LE scaling; the parameter is independent of the ligand size. LE_{scale} is estimated using equation (viii), and a LE_{scale} value lower than 0.4 suggests that the proposed compound may be potent against an enzyme.

$$LE_{scale} = 0.873 \times e^{-0.026 \times NHA} - 0.064 \quad \text{(viii)}$$

As seen in Table 3, the calculated Lescales for all molecules showed they are lower than 0.4; hence, they have the potential to inhibit KasA catalytic function.

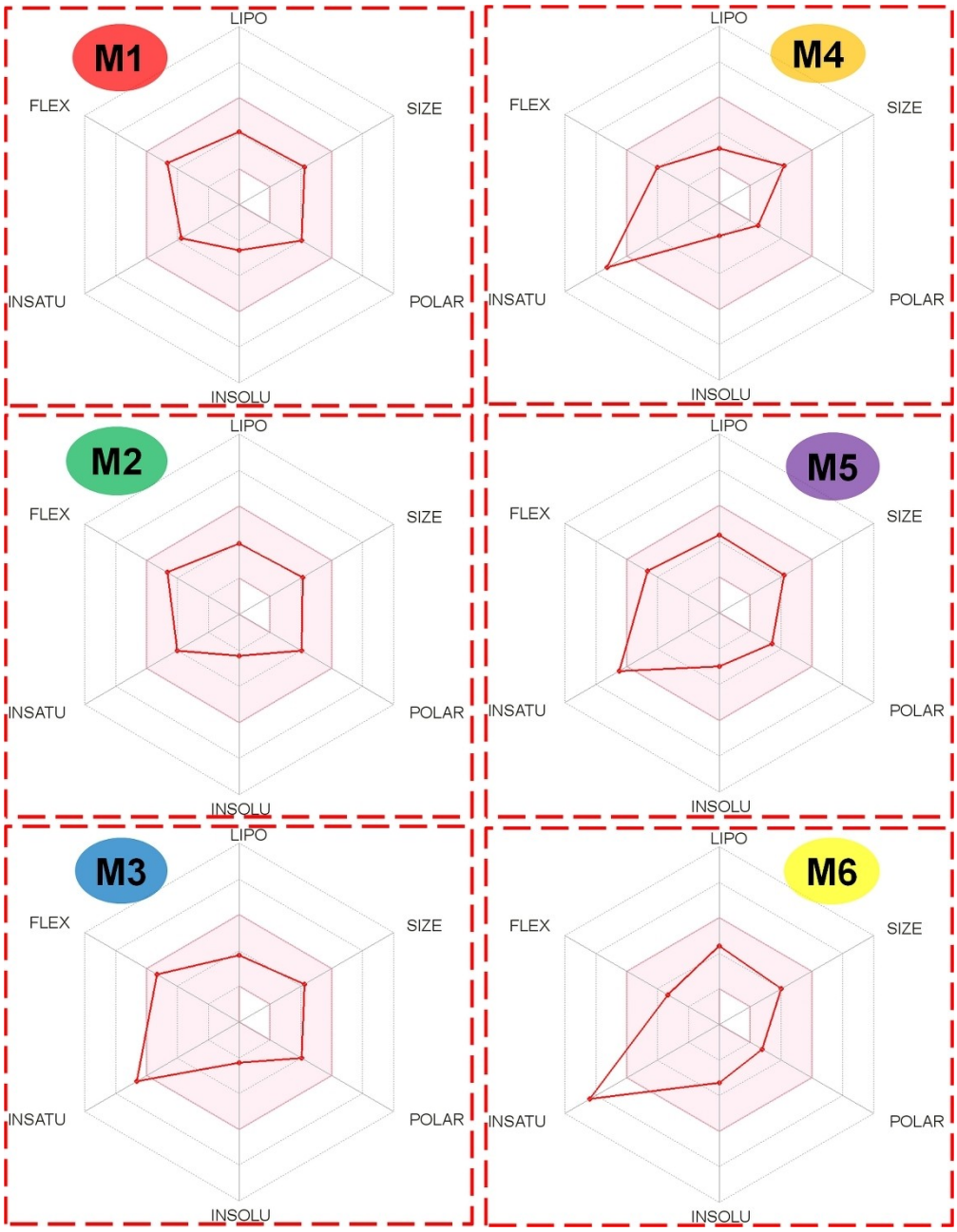

Figure 4. The plot of bioavailability radar for the final proposed *Mtb* KasA protein inhibitors M1, M2, M3, M4, M5, and M6.

Furthermore, we obtained fit quality (FQ) values for each proposed inhibitor of *Mtb* KasA protein. FQ is defined as the quotient of LE to LEscale, and the closer the calculated FQ value to 1, the stronger the ligand-receptor interaction. Individually, the FQ value for the proposed inhibitors is approximately 1. Interestingly, these values can be asserted to justify the need to investigate the inhibition of the KasA enzyme experimentally.

In the other to gain more insights into the inhibitory ligand potency, the ligand-efficiency-dependent lipophilicity (LELP) parameter was computed as follows in equation ix:

$$LELP = \frac{-BE}{LE} \quad \text{(ix)}$$

LELP parameter suggests that molecules optimize the affinity depending on lipophilicity. As seen in Table 3, the LELP value indicates that molecules M5 and M6 optimize the affinity due to lipophilicity. Perhaps, the molecules M1-M4 depended on the hydrophobicity of KasA active site residues.

Table 3. Predicted bioactivity and efficiency of the proposed *Mtb* KasA inhibitors.

Compound	BE[a]	K_i[b] (μM)	LE[c]	LE_{Scale}[d]	Fit Quality[e]	LELP[f]
M1	−10.4	0.2377	0.3852	0.3687	1.0448	0.2077
M2	−10.3	0.2814	0.3961	0.3800	1.0424	0.1515
M3	−10.3	0.2814	0.3815	0.3687	1.0347	0.3670
M4	−10.1	0.3944	0.3885	0.3800	1.0224	−0.3089
M5	−10.0	0.4669	0.3846	0.3800	1.0121	3.5101
M6	−10.0	0.4669	0.3846	0.3800	1.0121	3.8482

[a] Binding energy;
[b] Predicted inhibition constant;
[c] Ligand efficiency;
[d] Ligand efficiency scale;
[e] Fit quality;
[f] Ligand-effciency-dependent lipophilicity

Post-molecular dynamics analysis

Thermodynamics calculations of the screened molecules with KasA protein

The MM/GBSA method investigated the binding patterns and stabilization interactions of inhibitors M1 to M6 at the KasA active site by decomposing the binding free energies into inhibitor-residue pairs.[65] Post-dynamic calculations were carried out to determine the effect of the inhibitor binding to KasA using MM/GBSA method. The calculated binding free energies (BFE) of standard inhibitor TLM and the molecules are summarised in Table 4 below. As estimated, the BFE (kcal/mol) of JFX, M1, M2, M3, M4, M5, and M6 exhibited favourable binding energy compared to TLM's energy of −11.6924 kcal/mol as evidenced by their high negative energy (ΔG) values of −44.05, −35.9005, −33.4758, −32.5769, −39.5136, and −30.6634, respectively. The BFE of the TLM is 2-fold lower than the M6 (lowest among molecules' binding energies). M1 and M5 showed more binding affinity to KasA. Highly favourable van der Waals energies complemented their high ΔG values; −56.1845 kcal/mol and −51.9314 kcal/mol for KasA-M1 and KasA-M5, respectively. The free energy components were further explored separately to get insights into the driving forces between the compounds and their binding to KasA. The results suggest that both the intermolecular electrostatic and vdW interactions in the gas phase favour the binding of the inhibitors. A significant increase in vdW energy was observed with compound M1, which led to the increased binding affinity of KasA-M1.

Table 4. Summary of MMGB(PB)SA-based computed thermodynamics parameters obtained from the standard inhibitor (TLM)-KasA and the proposed molecules-KasA complexes.

	Complex							
Energy Component (kcal/mol)	KasA-TLM	KasA-JFX	KasA-M1	KasA-M2	KasA-M3	KasA-M4	KasA-M5	KasA-M6
ΔE_{vdW}[a]	−29.17 (±1.93)	−36.38 (±2.96)	−56.19 (±3.24)	−53.55 (±2.87)	−50.75 (±2.86)	−48.40 (±2.74)	−51.93 (±2.22)	−37.67 (±4.29)
ΔE_{elec}[b]	−234.43 (±8.49)	−41.12 (±4.54)	−15.59 (±6.95)	−14.12 (±5.03)	−18.11 (±6.43)	−20.93 (±8.64)	−19.96 (±3.95)	−12.50 (±6.96)
ΔG_{gas}[c]	−263.59 (±8.92)	−77.50 (±4.73)	−71.77 (±7.50)	−67.67 (±5.39)	−68.86 (±6.09)	−69.33 (±9.13)	−71.90 (±3.92)	−50.17 (±8.56)
E_{GB}[d]	255.70 (±8.35)	38.01 (±4.12)	36.67 (±4.31)	38.33 (±3.83)	41.62 (±3.54)	42.67 (±6.90)	38.37 (±2.60)	24.54 (±5.71)
E_{SA}[e]	−3.81 (±0.14)	−4.57 (±0.22)	−6.42 (±0.28)	−6.57 (±0.19)	−6.24 (±0.23)	−5.91 (±0.20)	−5.98 (±0.18)	−5.04 (±0.41)
ΔG_{solv}[f]	251.90 (±8.92)	33.44 (±4.08)	30.25 (±4.33)	31.76 (±3.81)	35.38 (±3.57)	36.58 (±6.86)	32.33 (±2.70)	19.50 (±5.53)
ΔG_{bind}[g]	−11.69 (±2.33)	−44.05 (±3.11)	−41.53 (±4.21)	−35.90 (±3.12)	−33.48 (±4.20)	−32.58 (±4.278)	−39.51 (±2.69)	−30.66 (±4.48)

[a] ΔE_{vdw} (van der Waals),
[b] ΔE_{elec} (Electrostatic),
[c] ΔG_{gas} (gas-phase energy),
[d] E_{GB} (Polar solvation energy),
[e] E_{SA}, Solvent-accessible surface area energy,
[f] ΔG_{solv} (Solvation free energy), and
[g] ΔG_{bind} (Calculated total free binding energy)

Inhibitor-KasA interaction landscape and per residue energy plot

The KasA residues that interacted with the JFX include LEU116 (−2.3 kcal/mol), ILE202 (−1.0 kcal/mol), PHE239 (−1.5 kcal/mol), ILE347 (−1.2 kcal/mol), and GLU199 (−0.3 kcal/mol). The residues contributed binding energies favour the strong binding JFX at the KasA active site, except GLU199. This finding correlates with the ΔG value of JFX-KasA mentioned above. Furthermore, we investigated the critical binding site residues and their respective roles in the differential binding of TLM, M1, M2, M3, M4, M5, and M6 towards KasA. Each complex's total binding free energy (ΔG) was decomposed into electrostatic, van der Waals and total energies using an MM/GBSA-integrated per-residue energy decomposition method. The residues that contributed the most energy values to TLM with their contributing energy (kcal/mol, in parentheses) include PRO278 (1.28), PHE400 (1.20), and GLY401 (1.20), while ALA285 (0.2), ALA319 (0.4), and PHE403 (0.4), contributed least energy values (Supplementary Figure S1). Figures 5 & 6 show crucial residues

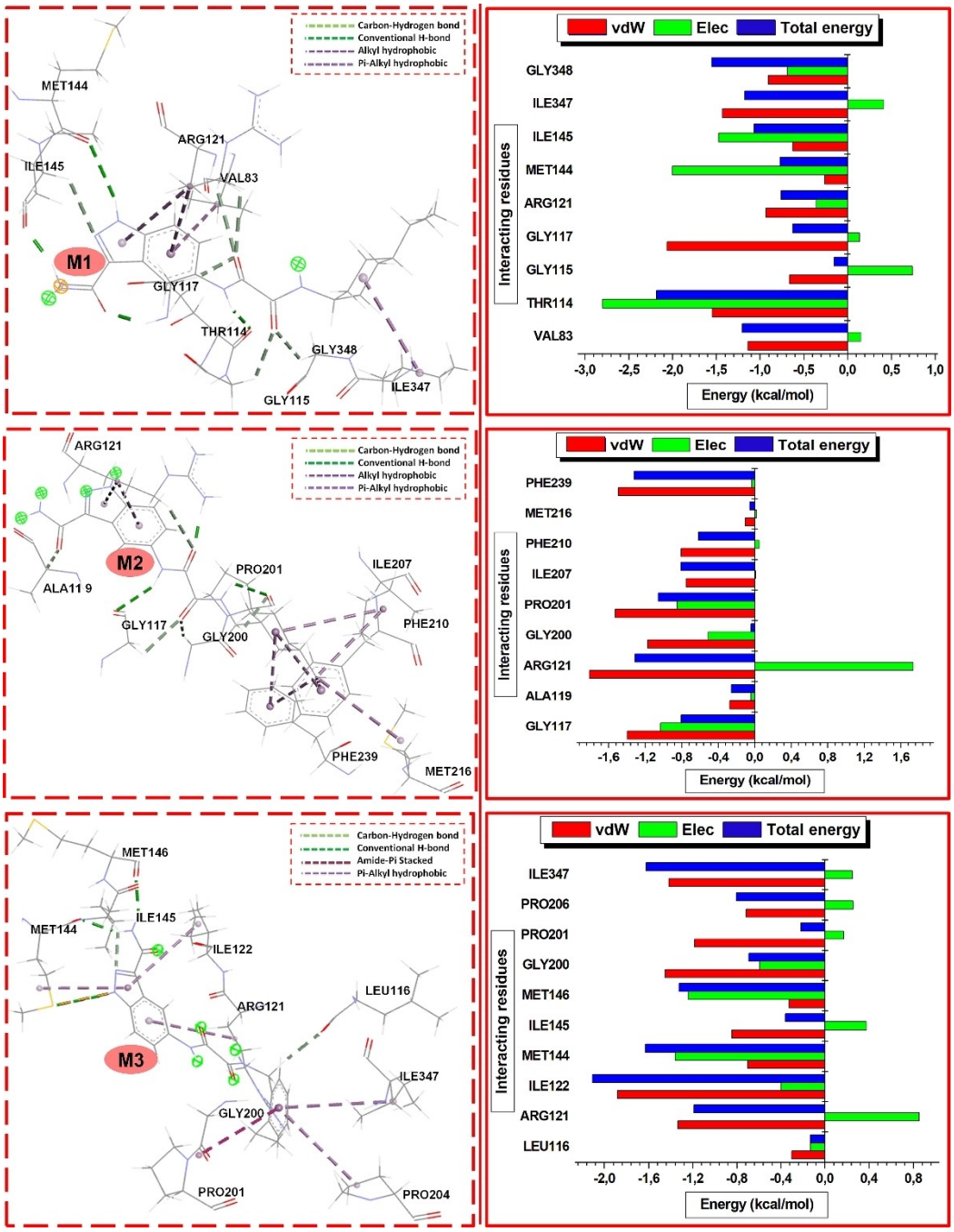

Figure 5. The binding landscape of proposed KasA enzyme inhibitors (M1, M2, and M3) in 3D surface view conformation and their respective per residue decomposition energy contributions

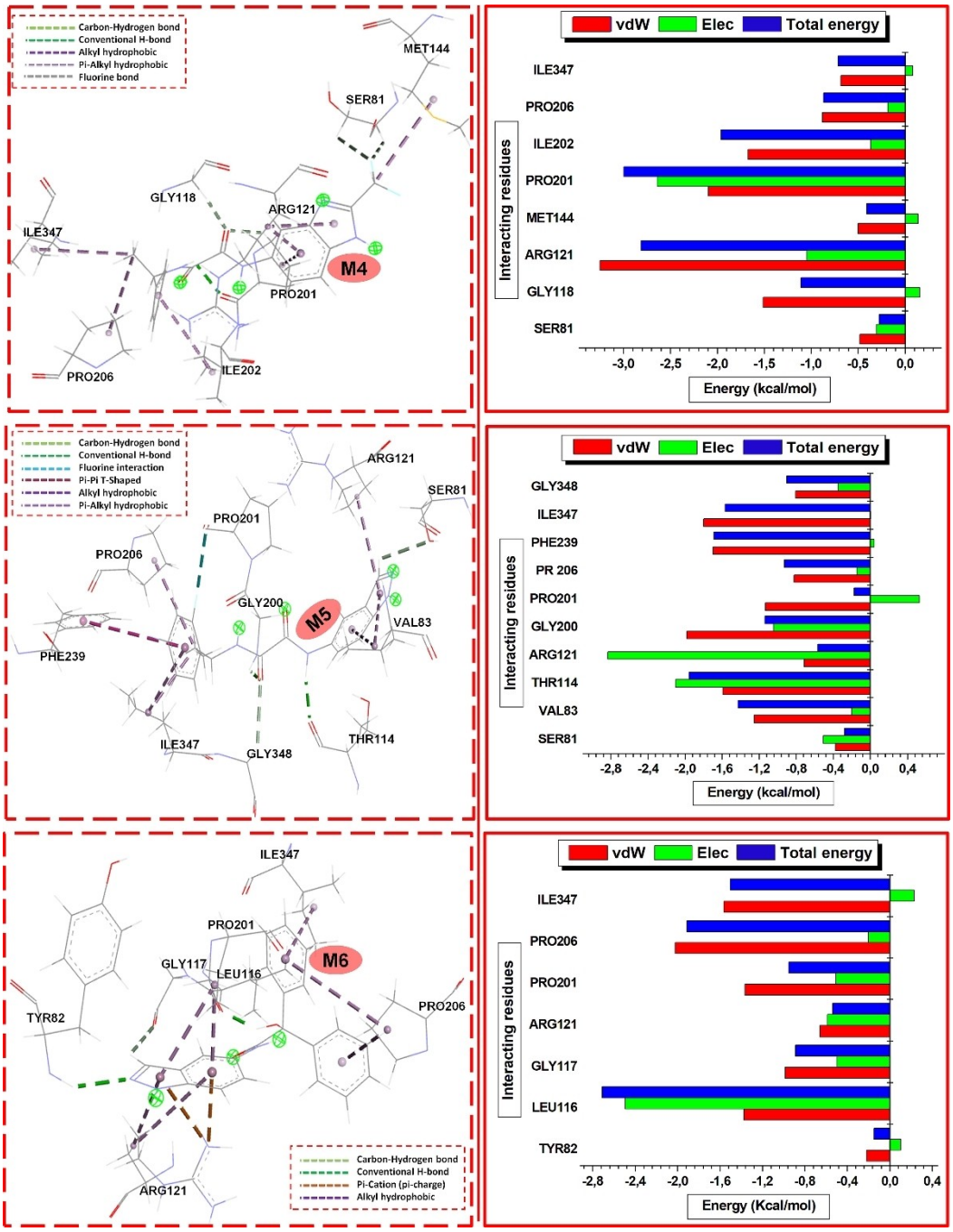

Figure 6. The binding landscape of the proposed KasA enzyme inhibitors (M4, M5, M6) in 3D surface view conformation and their respective per-residue decomposition energy contributions

that contributed to the binding free energies of the KasA-M1, KasA-M2, KasA-M3, KasA-M4, KasA-M5, and KasA-M6 complexes. The most favourable interactions originated predominantly from the residues that contributed binding energies of more than −1.0 kcal/mol. Figure 5 showed VAL83 (−1.1 kcal/mol), THR114 (−1.5 kcal/mol), GLY117 (−2.0 kcal/mol), ARG121 (−0.9 kcal/mol), ILE347 (−1.5 kcal/mol), GLY348 (−1.0 kcal/mol) in KasA-M1; GLY117 (−1.4 kcal/mol), ARG121 (−1.8 kcal/mol), GLY200 (−1.2 kcal/mol), PRO201 (−1.5 kcal/mol), ILE207 (−0.8 kcal/mol), PHE210 (−0.9 kcal/mol), PHE239 (−1.4 kcal/mol) in KasA-M2; and ARG121 (−1.4 kcal/mol), ILE122 (−1.8 kcal/mol), ILE145 (−0.8 kcal/mol), GLY200 (−1.4 kcal/mol), PRO201 (−1.2 kcal/mol), ILE347 (−1.4 kcal/mol) contributed in KasA-M3 system. Figure 6 showed that GLY118 (−1.5 kcal/mol), ARG121 (−3.2 kcal/mol), PRO201 (−2.0 kcal/mol), ILE202 (−1.7 kcal/mol), PRO206 (−0.8 kcal/mol) contributed in KasA-M4 complex; VAL83 (−1.2 kcal/mol), THR114 (−1.5 kcal/mol), GLY200 (−2.0 kcal/mol), PRO201 (−1.05 kcal/mol), PRO206 (−0.8 kcal/mol), PHE239 (−1.8 kcal/mol), ILE347 (−1.8 kcal/mol), GLY348 (0.8 kcal/mol) contributed in KasA-M5

complex; LEU116 (−1.3 kcal/mol), GLY117 (−1.0 kcal/mol), PRO201 (−1.4 kcal/mol), PRO206 (−2.0 kcal/mol), ILE347 (−1.6 kcal/mol) in KasA-M6 made predominant contributions to the binding free energy. Similarly, VAL83, THR114, ARG121, ILE347, and GLY348 residues contributed to KasA-M1 and KasA-M5 complex with the most energetic binding affinity. The similarity in the interacting residues between the two most energetic complexes was evident from their significant binding energy values different from other molecules (M2, M3, M4, and M6). Our findings showed that most binding pocket residues contributed immensely to the interactions through electrostatic and van der Waals forces. The binding energy seen in KasA-M1 and KasA-M5 was attributed majorly to elevated van der Waals and electrostatic interactions of M1 with Thr114 ($\Delta E_{vdW} = -1.6$ kcal/mol and $\Delta E_{elec} = -2.8$ kcal/mol) and M5 with Thr114 ($\Delta E_{vdW} = -1.6$ kcal/mol and $\Delta E_{elec} = -2.10$ kcal/mol).

The investigated inhibitors showed varying degrees of inhibitory potential as identified from the predicted inhibitory constants (K_i, Table 3) and binding energies (△G, Table 4), respectively. The chemical structures of the inhibitors M1, M2, M3, M4, M5, and M6 contain a pharmacologically important indazole scaffold.[66] The structural functionalities provide a possible justification for why these inhibitors showed therapeutic potential based on the findings in this study. From a medicinal chemistry point of view, the functional moieties of chemical structures (Figure 3) determine their potential therapeutic efficacies against infection or disease. They are essential factors in drug design and development.[67]

The nitrogen-containing heterocycles are necessary building blocks for many bioactive natural products and commercially available drugs. As pharmacologically crucial scaffolds, they have attracted considerable attention from chemists.[68] Indazoles are critical nitrogen-containing heterocyclic compounds with a bicyclic ring structure. The ring structure consists of pyrazole and benzene rings. Diverse substituted indazole derivatives have various functional groups and display versatile biological activities. Such activities include anti-inflammatory,[69] antiarrhythmic,[70] antitumor[71] antifungal,[72] anti-bacterial,[73] and anti-HIV[74] activities; hence, they have gained considerable attention in the field of medicinal chemistry.

Indazole moiety has previously been beneficial to increasing compounds' potency against *Mtb* and has contributed to the emergence of promising leads.[6] Therefore, it is plausible that indazole's presence in the structures of our investigated compounds is fundamentally responsible for the inhibitory potential recorded. However, the groups attached in the studied inhibitors' configurations can form differentially strong interactions with the active site of KasA. Thus, the different conformation of the compounds in the active region is enabled, possibly providing the reason for the varying degree of inhibition. For instance, the high electronegative atoms of these inhibitors can form strong bonding interactions with the interacting protein residues, thereby preventing the compound from moving in and out of the active site.[16]

Moreover, the oxygen atom of the carbonyl group, the hydrogen atom of the amide group, and the indazole rings can form strong conventional (carbon) hydrogen bonds, electrostatic, and pi-sigma interactions. Alkyl and mixed/pi-hydrophobic interactions between the inhibitors and the interacting residues can also form. By implication, differences between the six compounds are the Number of H-bond donor and acceptor groups, different ring systems, and topology.

The inhibitor M1-bound KasA is characterized by stable hydrophobic, halogen, and hydrogen bonds. For inhibitor M1, the system is characterized by stable hydrophobic and hydrogen bonds. Inhibitor M1 established pi-pi stacked interactions between GLY117 and the indazole ring. M1 also formed pi-pi staking interaction between the pyrazole ring and MET146. Moreover, Pi-alkyl interaction was formed between the phenyl ring of PHE239 and the C-atom of M1. It also formed a Pi-alkyl interaction between ARG121 and the pyrazole ring of indazole. Conventional H-bond was formed between the amine groups of compound M1 and the carbonyl O-atom of THR114, MET144, and ILE145.

The indazole resonating phenyl (C4-C9) ring of the compound M2 formed a strong pi-cation ARG121 side chain N atom. The pyrazole (N1-C5) ring of M2 also formed strong pi-anion interactions with the N atom of the ARG121 side chain. Conventional H-bond was formed between the H-atom side chain of Gly117 and the carbonyl oxygen (C-9) and between the H-atom of the pyrazole nitrogen (N1) Glu203. Pi-alkyl interactions between PRO201 and the resonating phenyl (C4-C9) and pyrazole (N1-C5) rings were observed in the indazole scaffold. Inhibitor M3 establishes pi-pi stacking interaction between its phenyl ring of the indazole scaffold (C14-C19) and Gly118; the pyrazole ring of compound 3 also interacts with Gly118, and the amine group performs conventional hydrogen interactions with Ser123, Met144, and Met146. It showed pi-alkyl interaction between the resonating phenyl ring and Pro204 and Ile345.

For the inhibitor M4, we observed strong pi-cation and pi-anion interactions between the phenyl ring of the indazole scaffold and Arg121; pyrazole and phenyl rings of the indazole formed pi-alkyl interaction with Arg121. Pi-alkyl interaction was also noticed between the phenyl ring and Ile202. The conventional hydrogen bond between the carbonyl O-atom of the compound and Gly118 was observed. A conventional H-bond between the amine group of the compound and PRO201 was seen.

The carbonyl O atoms of the GLY200, PRO201, and GLY240 formed strong and stable bonds with highly electronegative fluorine (F) atoms in the fluorobenzene ring of M5. The indazole scaffold's resonating phenyl (C4-C9) ring formed strong pi-pi stacked interactions differently with GLY117 and LEU116. The indazole, phenyl, and pyrazole rings also show pi-alkyl interaction with residue VAL83. Other significant interactions are the formation of conventional H-bonds formed from the backbones of LEU116 and SER81 with amide hydrogen (H-8) and pyrazole nitrogen (N-2) atoms of M5, respectively.

The inhibitor M6 has the least Number of interactions and formed pi-alkyl interactions: pyrazole ring and LEU205, phenyl rings with LEU116 and PRO206. A conventional H-bond was formed between the H-atom of the hydroxyl group of

compound M6 and the carbonyl O-atom of LEU116. The interactions between the hydrophobic active site residues enhance the binding and stability of the investigated inhibitors in the pocket. The ligands adopted favourable orientations interacting with the active site residues to form strong bonds through the indazole structural motifs –C=O, –NH, F, $-C_6H_5$ functional groups. These strong bonds and stability ensuring could be the reason for the inhibitory potential of the inhibitors against the KasA enzyme.

The functional groups directly fused to the pyrazole moiety of the indazole scaffold and as substituents attached to the structures' side chains provide the distinction between the JSF-3285 and the virtual screening inhibitors. For example, the methyl group at position C3, the sulphonamide group, and the alkylflouride in the structure of JSF-3285 are replaced by the carboxamide group, two secondary amides attached, and alkyl cyclohexane in M1. Similarly, the methyl group at position C3, the sulphonamide group, and the alkylflouride in the structure of JSF-3285 are replaced by a hydrogen atom, two secondary amides attached, and ortho, para-diflourobenzene. The presence and position of these substituents could potentially positively impact the development of these proposed inhibitors as anti-*Mtb* drugs. However, our MM/GBSA (detailed work not shown in this study) showed the binding energy of JSF-3285 ($\triangle G = -44.05$ kcal/mol) to be more energetically favourable than the proposed inhibitor, M1-M6 ($\triangle G$ ranging between −41.52 and −30.66 kcal/mol), which may or may not be significant.

Comparatively, the indazole moiety offers a central motif to JSF-3285 and the proposed inhibitors; however, it is assumed that the sulphonamide group present in the JSF-3285 structure impacts its binding energy greatly. Nevertheless, the presence of different electron-withdrawing groups within the structure of M1 ($\triangle G = -41.52$ kcal/mol) and M2 ($\triangle G = -39.53$ kcal/mol), for instance, which have the most favourable binding energy among the proposed inhibitors, could put the inhibitor in a vantage position as a more promising inhibitor of KasA enzyme compared to JSF-3285. In examining the indazole motif, the replacement of the methyl group (electron-donating) at position C3 in JSF-3285 by a carboxamide substituent (electron-withdrawing) on the pyrazole moiety in M1 and the increased electron-withdrawing inductive effect to the presence of difluorobenzene moiety in M5 offer the possibility for their increased interaction with the receptor. Notably, electron-withdrawing substituents have, in different studies, been implicated in enhancing the biological activities of indazole-containing compounds against various disease conditions, including cancer, inflammation, hypertension, and depression.[75–78]

The interesting physicochemical and PK parameters recorded for the proposed inhibitors in this study put them in a good standpoint as drug candidates in combating *Mtb*. Notably, the good solubility profiles of these inhibitors due to increased hydrogen bond interactions could put them on the frontline in anti-*Mtb* drug discovery programs. In addition, the indazole scaffold played a prominent role in forming hydrogen bonds with critical protein residues. Then, the electron-withdrawing substituents in the proposed inhibitors furnished favourable hydrophilic interactions for this scaffold regarding its size, reactivity, and orientation. Again, secondary amide substituents in these inhibitors could be responsible for their good solubility profiles.

The presence of electron-withdrawing substituents in the proposed inhibitors furnished a favourable hydrophilic interaction for this scaffold regarding its size, reactivity, and orientation. Again, secondary amide substituents in these inhibitors could be responsible for their good solubility profiles. The introduction of electron-withdrawing substituents into indazole-containing compounds has been reported to improve oral bioavailability in cardiovascular disease, inhibiting transmyocardial laser revascularisation (TMLR).[39] Therefore, it is plausible that the increased electron-withdrawing groups present in these proposed inhibitors afforded them the good bioavailability scores recorded. Fluorine can improve permeability by modulation of molecule lipophilicity, reduction of amine basicity, or directing fluorine-protein interactions.[79] Therefore, incorporating fluorine at different positions of M4 and M5 could potentially increase their permeability. This assertion agrees with the partition coefficient, lipophilicity, and bioavailability score results of the proposed inhibitors in this study. Consequently, these proposed inhibitors could favour optimization through rational synthesis or modification capable of enhancing biological activities towards a robust anti-*Mtb* drug discovery program.

Protein stability, flexibility, and compactness

The C-α RMSD, C-α RMSF, and C-α RoG values of backbone atoms due to their starting structures can appropriately evaluate the stability of a 3D protein structure. For this reason, we can understand the dynamics and equilibrium of the protein structures. In this respect, the variations in the residue positions were explored by calculating RMSD, RMSF, and RoG across the duration of the MD simulation. The mean RMSD values of the apo and JFX-KasA systems were 2.80 Å and 2.52 Å, respectively. The RMSD plots in Figure 7C show convergence of the overall structure at approximately 80 ns. Figure 7C shows that the RMSD of all the bound systems was lower than that of the unbound system throughout the simulation time, which correlates with the average RMSD values (Table 5). This observation may indicate that the compounds stabilize the protein's active site. However, the KasA-TLM (1.55 Å) and KasA-M1 (1.57 Å) systems showed much lower average RMSD among all bound systems, signifying the most stable structures relative to other inhibitors-bound enzymes. Thus, it indicates that the binding of M1 has a more stabilizing effect on the binding domain than other inhibitors. The highly stable binding pocket residues observed in M1-bounding could favour an increased residual interaction with M1, leading to stronger binding to KasA than other inhibitors.

Furthermore, the average RMSF value of KasA-JFX was 1.04 Å, which is still within the expected difference result compared to the RMSF of the Apo system. The average RMSF values in Table 5 revealed the highest fluctuation in the

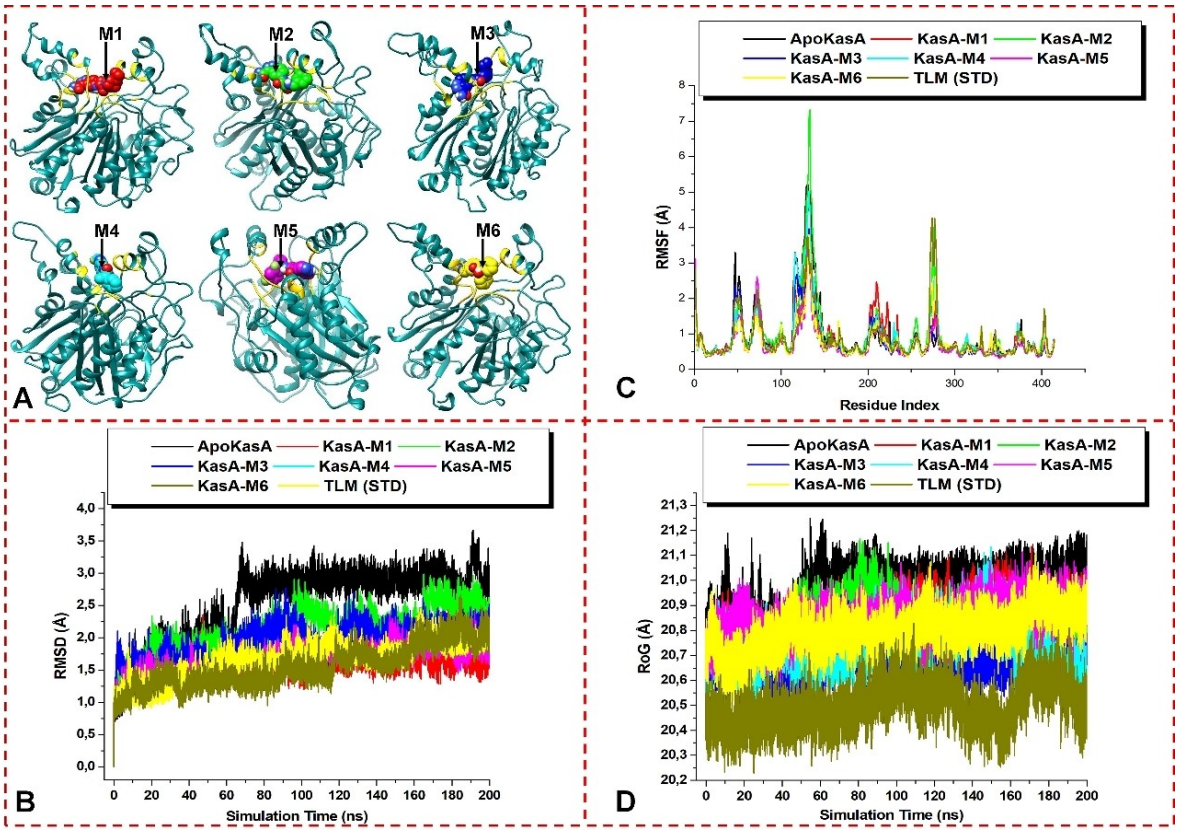

Figure 7. (A) The inhibitors: M1 (red), M2 (green), M3 (blue), M4 (cyan), M5 (pink) and M6 (yellow) bound to KasA active site. The plots of RMSF (B), RMSD (C), and RoG (D) of unbound, TLM-bound and the proposed molecules-bound systems were computed after 200 ns simulation time.

Table 5. Maximum, Minimum, and Mean RMSD, RMSF, and radius of gyration (RoG) of the Apo and potential inhibitors-bound KasA systems.

Complex	RMSD (Å)		RMSF (Å)		RoG (Å)	
	Mean	SD ±	Mean	SD ±	Mean	SD ±
ApoKasA	2.88	0.51	0.94	0.81	20.97	0.82
KasA-TLM	1.55	0.32	0.88	0.66	20.50	0.08
KasA-M1	1.57	0.17	0.87	0.55	20.82	0.07
KasA-M2	2.35	0.42	0.99	0.86	20.80	0.08
KasA-M3	1.97	0.42	0.79	0.56	20.69	0.06
KasA-M4	1.71	0.23	0.87	0.70	20.69	0.12
KasA-M5	1.71	0.23	0.72	0.47	20.85	0.07
KasA-M6	1.66	0.28	0.77	0.46	20.79	0.07

unbound system (0.94 Å) compared to the bound systems, indicating that the fluctuation reduced upon the binding of the inhibitors except for the KasA-M2 (0.99 Å), which showed higher instability than all systems. Figure 7B also showed highly fluctuated residues of the unbound enzyme relative to the investigated inhibitors. Thus, it suggested that the original structure of KasA generally consists of highly flexible residues which become rigid upon inhibitor binding. This notable reduction can be correlated to structural inactivation, presumably due to stronger high-affinity interactions of the inhibitors at the KasA active site. The reduced residue flexibility observed in the inhibitor-bound structures suggests that the functional moiety present in these inhibitors possibly induced a stronger restricted motion of individual residues relative to the unbound enzyme. The restricted residue fluctuation could have led to KasA inhibition.

In addition, the RoG of the unbound enzyme and the inhibitor-bound KasA were also calculated to measure the entire protein structure's compactness throughout the simulation. Table 5 and Figure 7D show that the unbound structure possesses the highest average RoG value relative to all bound KasA structures. The possible indication is that the protein's active site exhibited increased structural compactness when bound to the inhibitors. The lower RoG of the inhibitors bound KasA indicates that the binding of the inhibitors resulted in tighter KasA conformation than the unbound system. There-

fore, KasA-TLM is the most compact complex among the bound systems. These findings corroborate the above RMSD and RMSF results.

Principle component analysis (PCA)

Finally, the principal component analysis was computed for the proposed molecule-bound structures to understand the atomic motion among the interstitial residues of KasA protein upon inhibitor binding. The molecules' interactions and inhibition mechanisms were investigated by computing the first two components (PC1 and PC2) of the principal component analysis (PCA). The study helps identify the most strongly correlated variables with each element or the numbers with the large magnitude farthest from zero in either direction.[40] The level at which a correlation is essential is determined. A correlation above a given value may be deemed necessary. PCA reveals the displacement of the KasA C-α atoms during MD simulations performed using the CPPTRAJ in AMBER18 GPU.

The MD simulation's convergence in space was obtained using the Cartesian coordinates from the averaged structure covariance matrix. PC1 was plotted along the vertical axis, and PC2 was plotted along the horizontal axis, which indicates the covariance matrix after eigenvector elimination. The protein motion shifts along specific directions were represented by eigenvectors, given by the normal mode. Single-directional motion relative to each point was uniquely Oriented because of the overlapping of typical structures. Figure 8 illustrates the scatter plot generated by the unbound KasA (black), KasA-M1 (red), KasA-M2 (green), KasA-M3 (blue), KasA-M4 (cyan), KasA-M5 (purple), and KasA-M6 (yellow).

The plot showed distinct conformations and motions in the essential subspace along the two principal components. The apo system showed inter-residual displacement along the eigenvectors, but the bound systems revealed a more apparent motion separation among the seven systems. The KasA-M2 and KasA-M5 displayed the most dispersed motion along the two eigenvectors. The M2 and M5 molecules could indicate enhanced structural activity upon binding to the KasA enzyme

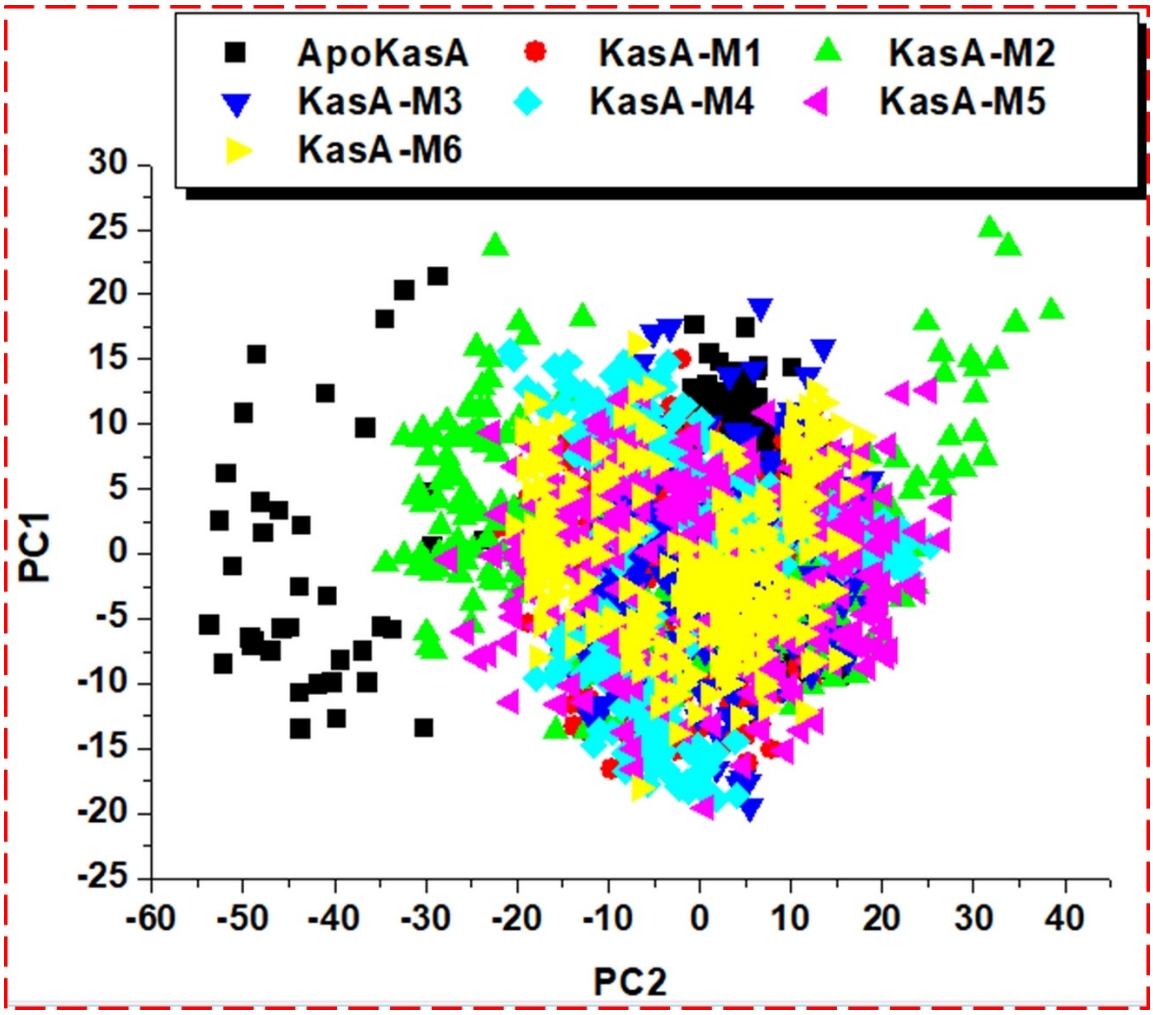

Figure 8. PCA of the C-α backbone atoms for ApoKasA, M1-, M2-, M3-, M4-, M5- and M6-bound KasA conformations along the PC1 and PC2 principal components during the 200 ns MD simulation.

compared to the M1, M3, M4, and M6, representing compact motions. These insights corroborate the above-discussed results, which collectively show that the binding of the proposed molecules stabilized a high active conformation favouring the inhibition of KasA enzymatic activity.

Conclusion

Structure-based virtual screening (SBVS) is integral to rational drug design. SBVS yielded 817 antimycobacterial molecules in this study during a search from the ZINCPharmer chemical libraries. The molecular compounds underwent a series of computer-based drug design screenings that produced six final potential KasA inhibitors. The prospective chemotypes can provide an avenue to discover future antibacterial drugs based on their promising results. The six screened inhibitors produced higher binding affinities and predicted bioactivity for KasA active site compared to thiolactomycin. Moreover, an integrated molecular dynamics simulation was performed to assess the stability, flexibility, and compactness of KasA protein upon the binding of the ligands. The proposed SBVS KasA inhibitors in this work have antimycobacterial activities and can be validated using wet lab-based experimental techniques.

Supporting Information

Figure S1. Per-residue decomposition plot shows the KasA protein's energy contributions to the standard inhibitor (TLM) interaction.

Disclosure

The molecular dynamics simulation and the binding free energy methodology used in this study were the modified procedure applied in a previously published "Nature-Inspired O-Benzyl Oxime-Based Derivatives as New Dual-Acting Agents Targeting Aldose Reductase and Oxidative Stress" article. Although there may be a few similarities in the text, the authors unanimously stated that the published work is entirely different and not a part of this study.

Declaration

The authors provide the editors with the approval to include sub-headings and other headings in this manuscript.

Acknowledgements

The authors acknowledge the Centre for High-Performance Computing, Cape Town, for providing computational resources.

Conflict of Interest

The authors declare no conflict of interest.

Data Availability Statement

Data sharing is not applicable to this article as no new data were created or analyzed in this study.

Keywords: tuberculosis · enzyme inhibitors · molecular informatics · MD simulations · bioactivity

[1] World Health Organization, *WHO Global Tuberculosis Report, 2021*, **2021**.
[2] M. Holzheimer, A. J. Minnaard, *Chem. Rev.* **2021**, *121*, 9554–9643.
[3] A. J. Zimmer, J. S. Klinton, C. Oga-Omenka, P. Heitkamp, C. Nawina Nyirenda, J. Furin, M. Pai, *J. Epidemiol. Community Health* **2022**, *76*, 310–316.
[4] M. Pai, T. Kasaeva, S. Swaminathan, *N. Engl. J. Med.* **2022**, *386*, 1490–1493.
[5] H. G. Mamatha, V. Shanthi, *J. Glob. Antimicrob. Resist.* **2018**, *12*, 5–10.
[6] P. Kumar, G. C. Capodagli, D. Awasthi, R. Shrestha, K. Maharaja, P. Sukheja, S. G. Li, D. Inoyama, M. Zimmerman, H. P. H. Liang, J. Sarathy, M. Mina, G. Rasic, R. Russo, A. L. Perryman, T. Richmann, A. Gupta, E. Singleton, S. Verma, S. Husain, P. Soteropoulos, Z. Wang, R. Morris, G. Porter, G. Agnihotri, P. Salgame, S. Ekins, K. Y. Rhee, N. Connell, V. Dartois, M. B. Neiditch, J. S. Freundlich, D. Alland, *mBio* **2018**, *9*, 1–23.
[7] L. Kremer, J. D. Douglas, R. Alain, C. Morehouse, M. R. Guy, D. Alland, L. G. Dover, H. Jeremy, W. R. Jacobs, J. Patrick, D. E. Minnikin, S. Gurdyal, *J. Biol. Chem.* **2000**, *22*, 16857–16864.
[8] A. K. Brown, R. C. Taylor, A. Bhatt, K. Fu, *PLoS One* **2009**, *4*, e6306.
[9] J. Schiebel, K. Kapilashrami, A. Fekete, G. R. Bommineni, C. M. Schaefer, M. J. Mueller, P. J. Tonge, C. Kisker, *J. Biol. Chem.* **2013**, *288*, 34190–34204.
[10] S. Oh, L. Trifonov, V. D. Yadav, C. E. B. Iii, H. I. Boshoff, *Front. Cell. Infect. Microbiol.* **2021**, *11*, 1–23.
[11] C. A. Machutta, G. R. Bommineni, S. R. Luckner, K. Kapilashrami, B. Ruzsicska, C. Simmerling, C. Kisker, P. J. Tonge, *J. Biol. Chem.* **2010**, *285*, 6161–6169.
[12] D. Inoyama, D. Awasthi, G. C. Capodagli, K. Tsotetsi, P. Sukheja, M. Zimmerman, S.-G. Li, R. Jadhav, R. Russo, X. Wang, C. Grady, T. Richmann, R. Shrestha, L. Li, Y.-M. Ahn, H. P. Ho Liang, M. Mina, S. Park, D. S. Perlin, N. Connell, V. Dartois, D. Alland, M. B. Neiditch, P. Kumar, J. S. Freundlich, *Cell Chem. Biol.* **2020**, 1–11.
[13] X. Lin, X. Li, X. Lin, *Molecules* **2020**, *25*, 1–17.
[14] M. A. Ejalonibu, S. A. Ogundare, A. A. Elrashedy, M. A. Ejalonibu, M. M. Lawal, N. N. Mhlongo, H. M. Kumalo, *Int. J. Mol. Sci.* **2021**, *22*, 1–39.
[15] M. K. Thirunavukkarasu, R. Karuppasamy, *J. Biomol. Struct. Dyn.* **2021**, *0*, 1–12.
[16] A. T. Adewumi, O. S. Soremekun, M. B. Ajadi, M. E. S. Soliman, *RSC Adv.* **2020**, *10*, 23466–23483.
[17] P. Ramharack, M. E. S. Soliman, *J. Biomol. Struct. Dyn.* **2018**, *36*, 1118–1133.
[18] C. S. Jangam, S. Bhowmick, R. D. Chorge, L. D. Bharatrao, P. C. Patil, R. V. Chikhale, N. A. AlFaris, J. zaidan ALTamimi, S. M. Wabaidur, M. A. Islam, *Comput. Biol. Chem.* **2019**, *83*, 107136.
[19] A. T. Adewumi, A. Elrashedy, O. S. Soremekun, M. B. Ajadi, M. E. S. Soliman, *J. Biomol. Struct. Dyn.* **2022**, *40*, 2934–2954.
[20] W. M. Oluyemi, B. B. Samuel, A. T. Adewumi, Y. A. Adekunle, M. E. S. Soliman, L. Krenn, *Chem. Biodiversity* **2022**, *19*, 1–20.
[21] A. Daina, O. Michielin, V. Zoete, *Sci. Rep.* **2017**, *7*, 1–13.
[22] A. Daina, O. Michielin, V. Zoete, *J. Chem. Inf. Model.* **2014**, *54*, 3284–3301.
[23] E. F. Pettersen, T. D. Goddard, C. C. Huang, G. S. Couch, D. M. Greenblatt, E. C. Meng, T. E. Ferrin, *J. Comput. Chem.* **2004**, *25*, 1605–1612.
[24] A. T. Adewumi, P. Ramharack, O. S. Soremekun, M. E. S. Soliman, *Protein J.* **2020**, *39*, 118–132.
[25] A. J. O. Garrett, M. Morris, Ruth Huey, W. Lindstrom, M. F. Sanner, R. K. Belew, D. S. Goodsell, *J. Comput. Chem.* **2009**, *30*, 2785–2791.
[26] R. Thomsen, M. H. Christensen, *J. Med. Chem.* **2006**, *49*, 3315–3321.
[27] O. S. Soremekun, K. F. Omolabi, A. T. Adewumi, *Futur. Sci. OA* **2020**, *7*, 1–10.
[28] D. R. Koes, C. J. Camacho, *Nucleic Acids Res.* **2012**, *40*, 409–414.
[29] L. Heo, W. H. Shin, M. S. Lee, C. Seok, *Nucleic Acids Res.* **2014**, *42*, 210–214.

[30] O. Trott, A. J. Olson, *J. Comput. Chem.* **2010**, *31*, 455–461.
[31] L. G. Ferreira, R. N. Dos Santos, G. Oliva, A. D. Andricopulo, *Molecules* **2015**, *20(7)*, 13384–13421
[32] D. Mucs, R. A. Bryce, *Expert Opin. Drug Discovery* **2013**, *8*, 263–276.
[33] S. Chetty, M. E. S. Soliman, *Med. Chem. Res.* **2015**, *24*, 2055–2074.
[34] T. S. Lee, D. S. Cerutti, D. Mermelstein, C. Lin, S. Legrand, T. J. Giese, A. Roitberg, D. A. Case, R. C. Walker, D. M. York, *J. Chem. Inf. Model.* **2018**, *58*, 2043–2050.
[35] D. A. Case, T. E. Cheatham, T. Darden, H. Gohlke, R. Luo, K. M. Merz, A. Onufriev, C. Simmerling, B. Wang, R. J. Woods, *J. Comput. Chem.* **2005**, *26*, 1668–1688.
[36] S. Zheng, Q. Tang, J. He, S. Du, S. Xu, C. Wang, Y. Xu, F. Lin, *J. Chem. Inf. Model.* **2016**, *56*, 811–818.
[37] P. Florova, P. Sklenovsky, P. Bana, *J. Chem. Theory Comput.* **2010**, *6*, 3569–3579.
[38] J. P. Ryckaert, G. Ciccotti, H. J. C. Berendsen, *J. Comput. Phys.* **1977**, *23*, 327–341.
[39] Y. Dong, M. Liao, X. Meng, G. N. Somero, *Proc. Nat. Acad. Sci.* **2018**, *115*, 1274–1279.
[40] M. Post, S. Wolf, G. Stock, *J. Chem. Phys.* **2019**, *150*, 1–11.
[41] S. Genheden, U. Ryde, *Expert Opin. Drug Discovery* **2015**, *10*, 449–461.
[42] V. Gapsys, L. S. Michielssens, J. H. Peters, B. L. de Groot, H. Leonov, *Methods Mol. Biol.* **2015**, *1215*, 173–209.
[43] A. T. Adewumi, A. Elrashedy, O. S. Soremekun, M. B. Ajadi, M. E. S. Soliman, *J. Biomol. Struct. Dyn.* **2020**, *40*, 1–21.
[44] E. Lionta, G. Spyrou, D. Vassilatis, Z. Cournia, *Curr. Top. Med. Chem.* **2014**, *14*, 1923–1938.
[45] S. R. Luckner, C. A. Machutta, P. J. Tonge, C. Kisker, *Structure* **2009**, *17*, 1004–1013.
[46] M. Kumari, N. Subbarao, *J. Biomol. Struct. Dyn.* **2019**, *38*, 5062-5080.
[47] M. Athar, A. N. Sona, B. D. Bekono, F. Ntie-Kang, *Phys. Sci. Rev.* **2019**, *4*, 20180101
[48] Í. F. Protti, D. R. Rodrigues, S. K. Fonseca, R. J. Alves, *ChemMedChem* **2021**, *16*, 1446–1456.
[49] D. F. Veber, S. R. Johnson, H. Y. Cheng, B. R. Smith, K. W. Ward, K. D. Kopple, *J. Med. Chem.* **2002**, *45*, 2615–2623.
[50] N. J. Sadgrove, G. L. Jones, *Curr. Pharmacother. Paradig. Nat. Antimicrob.* **2019**, *10*, 1–26.
[51] K. Pathak, S. Raghuvanshi, *Clin. Pharmacokinet.* **2015**, *54*, 325–357.
[52] J. V. Turner, D. J. Maddalena, S. Agatonovic-Kustrin, *Pharm. Res.* **2004**, *21*, 68–82.
[53] P. Gao, M. E. Guyton, T. Huang, J. M. Bauer, K. J. Stefanski, Q. Lu, *Drug Dev. Ind. Pharm.* **2004**, *30*, 221–229.
[54] N. Kanikkannan, *J. Anal. Pharm. Res.* **2018**, *7*, 45–50.
[55] P. Ertl, A. Schuffenhauer, *J. Cheminf.* **2009**, *1*, 1–11.
[56] B. Li, H. Chen, *Molecules* **2022**, *27*, 1–17.
[57] D. Lagorce, D. Douguet, M. A. Miteva, B. O. Villoutreix, *Sci. Rep.* **2017**, *7*, 1–15.
[58] H. Pajouhesh, G. R. Lenz, *J. Am. Soc. Exp. Neurother.* **2005**, *2*, 541–553.
[59] S. A. Hitchcock, L. D. Pennington, *J. Med. Chem.* **2006**, *49*, 7559–7583.
[60] M. J. Jedrzejas, S. Singh, W. J. Brouillette, G. M. Air, M. Luo, *Proteins Struct. Funct. Bioinf.* **1995**, *23*, 264–277.
[61] J. P. Hughes, S. S. Rees, S. B. Kalindjian, K. L. Philpott, *Br. J. Pharmacol.* **2011**, *162*, 1239–1249.
[62] C. H. Reynolds, R. C. Reynolds, *J. Chem. Inf. Model.* **2017**, *57*, 3086–3093.
[63] A. L. Hopkins, C. R. Groom, A. Alex, *Drug Discovery Today* **2004**, *9*, 430–431.
[64] C. H. Reynolds, S. D. Bembenek, B. A. Tounge, *Bioorg. Med. Chem. Lett.* **2007**, *17*, 4258–4261.
[65] F. B. Akher, A. Farrokhzadeh, F. A. Olotu, C. Agoni, M. E. S. Soliman, *Org. Biomol. Chem.* **2019**, *17*, 1176–1190.
[66] S. G. Zhang, C. G. Liang, W. H. Zhang, *Molecules* **2018**, *23(11)*, 2783.
[67] D. Awasthi, K. Kumar, S. E. Knudson, R. A. Slayden, I. Ojima, *J. Med. Chem.* **2013**, *56*, 9756–9770.
[68] M. Gao, B. Xu, *Chem. Rec.* **2016**, *16*, 1701–1714.
[69] S. Vidyacharan, A. Murugan, D. S. Sharada, *J. Org. Chem.* **2016**, 2837–2848.
[70] A. H. Shinde, S. Vidyacharan, D. S. Sharada, *Org. Biomol. Chem.* **2016**, *14*, 3207–3211.
[71] S. Behrouz, *J. Heterocycl. Chem.* **2017**, *54*, 1863–1871.
[72] M. Jayanthi, P. Rajakumar, *J. Heterocycl. Chem.* **2017**, *54*, 3042–3050.
[73] H. Lavrard, F. Popowycz, *Synthesis* **2018**, *50*, 998–1006.
[74] G. Bogonda, H. Y. Kim, K. Oh, *Org. Lett.* **2018**, *20*, 2711–2215.
[75] H. Schleifer, B. Doleschal, M. Lichtenegger, R. Oppenrieder, I. Derler, *Br. J. Pharmacol.* **2012**, *167*, 1712–22.
[76] I. Gameiro, P. Michalska, G. Tenti, Á. Cores, I. Buendia, A. I. Rojo, N. D. Georgakopoulos, J. M. Hernández-guijo, M. T. Ramos, G. Wells, M. G. López, A. Cuadrado, J. C. Menéndez, R. León, *Sci. Rep.* **2017**, *7*, 1–15.
[77] R. Kenchappa, Y. D. Bodke, *Chem. Data Collect.* **2020**, *28*, 100453.
[78] R. F. Costa, L. C. Turones, K. Valéria, N. Cavalcante, I. Aureliano, R. Júnior, C. H. Xavier, L. P. Rosseto, H. B. Napolitano, P. Ferreira, M. Luiz, F. Neto, G. M. Galvão, R. Menegatti, G. R. Pedrino, E. A. Costa, J. Luis, R. Martins, J. O. Fajemiroye, *Front. Pharmacol.* **2021**, *12*, 1–9.
[79] J. Cui, X. Peng, D. Gao, Y. Dai, J. Ai, Y. Li, *Bioorg. Med. Chem. Lett.* **2017**, *27*, 3782–3786.

Submitted: October 5, 2022
Accepted: December 14, 2022